Molecular Therapy
Original Article

A Blood-Brain-Barrier-Penetrating Anti-human Transferrin Receptor Antibody Fusion Protein for Neuronopathic Mucopolysaccharidosis II

Hiroyuki Sonoda,[1,3] Hideto Morimoto,[1] Eiji Yoden,[1] Yuri Koshimura,[1] Masafumi Kinoshita,[1] Galina Golovina,[1] Haruna Takagi,[1] Ryuji Yamamoto,[1] Kohtaro Minami,[1] Akira Mizoguchi,[2] Katsuhiko Tachibana,[1] Tohru Hirato,[1] and Kenichi Takahashi[1,3]

[1]Research Division, JCR Pharmaceuticals, Kobe, Japan; [2]Department of Neural Regeneration and Cell Communication, Mie University Graduate School of Medicine, Tsu, Japan

Mucopolysaccharidosis II (MPS II) is an X-linked recessive lysosomal storage disease caused by mutations in the iduronate-2-sulfatase (*IDS*) gene. Since IDS catalyzes the degradation of glycosaminoglycans (GAGs), deficiency in this enzyme leads to accumulation of GAGs in most cells in all tissues and organs, resulting in severe somatic and neurological disorders. Although enzyme replacement therapy with human IDS (hIDS) has been used for the treatment of MPS II, this therapy is not effective for defects in the CNS mainly because the enzyme cannot cross the blood-brain barrier (BBB). Here, we developed a BBB-penetrating fusion protein, JR-141, which consists of an anti-human transferrin receptor (hTfR) antibody and intact hIDS. The TfR-mediated incorporation of JR-141 was confirmed by using human fibroblasts *in vitro*. When administrated intravenously to hTfR knockin mice or monkeys, JR-141, but not naked hIDS, was detected in the brain. In addition, the intravenous administration of JR-141 reduced the accumulation of GAGs both in the peripheral tissues and in the brain of hTfR knockin mice lacking *Ids*, an animal model of MPS II. These data provide a proof of concept for the translation of JR-141 to clinical study for the treatment of patients with MPS II with CNS disorders.

INTRODUCTION

Lysosomal storage diseases (LSDs) are a class of more than 50 distinct inherited metabolic diseases caused by deficiency of a particular lysosomal protein, with global incidence of approximately 1 in 8,000 live births.[1] Among LSDs, Mucopolysaccharidosis II (MPS II), also known as Hunter syndrome, is an X-linked recessive disorder,[2] hence girls are affected only rarely. MPS II is caused by a deficiency of iduronate-2-sulfatase (IDS), which is an essential enzyme for the degradation of lysosomal glycosaminoglycans (GAGs), such as heparan sulfate and dermatan sulfate.[2–4] Loss of IDS activity leads to pathological accumulation of GAGs in most cells in all tissues and organs, resulting in a broad spectrum of symptoms, including coarse facial features, skeletal deformities, joint stiffness, recurrent respiratory infections, hepatosplenomegaly, cardiac failure, renal degeneration, and deafness[1–4]. Severe forms of the disease are characterized by progressive deterioration of CNS function, manifested as cognitive impairment.[5] There is an ethnic variation in the incidence of MPS II: the numbers reported are 0.13, 0.27, 0.27, 0.31, 0.46, 0.64, 0.71, 0.84, and 1.07 cases per 100,000 newborns in Norway,[6] Sweden,[6] Denmark,[6] Western Australia,[7] Switzerland,[8] Germany,[9] Northern Ireland,[10] Japan,[8] and Taiwan,[11] respectively.

Enzyme replacement therapy (ERT) has been developed for the treatment of LSDs including MPS II.[12] This therapeutic approach depends on the delivery of intravenously injected recombinant enzymes to cell-surface receptors of the affected tissues and organs. Delivery of the intravenously injected lysosomal enzymes to cells employs mainly the cation-independent mannose 6-phosphate receptor (M6PR), which recognizes mannose 6-phosphate (M6P) moieties present on the carbohydrate chains of the enzymes.[13] ERT for MPS II by human IDS (hIDS) has been reported to improve the symptoms, including endurance, joint mobility, pulmonary function, swelling of the liver, and spleen, and to reduce the urinary excretion of GAGs.[14–18] However, the current ERT for MPS II does not work well in the bone, cornea, and cardiac valves.[19] In addition, a major drawback of this therapy is the inability to prevent or improve CNS manifestations,[14,15] mainly because the recombinant hIDS cannot be delivered to the brain due to the presence of the blood-brain barrier (BBB).

The BBB is formed by a continuous monolayer of brain capillary endothelial cells, the basement membrane, and astrocytes.[20] Although the tight junctions of the endothelial cells block the passage of large molecules, some endogenous proteins, including insulin, leptin, and

Received 14 December 2017; accepted 21 February 2018;
https://doi.org/10.1016/j.ymthe.2018.02.032.

[3]These authors contributed equally to this work.

Correspondence: Hiroyuki Sonoda, Research Division, JCR Pharmaceuticals, 2-2-9 Murotani, Nishi-ku, Kobe 651-2241, Japan.
E-mail: sonoda-h@jcrpharm.co.jp
Correspondence: Kenichi Takahashi, Research Division, JCR Pharmaceuticals, 2-2-9 Murotani, Nishi-ku, Kobe 651-2241, Japan.
E-mail: takahasi@jcrpharm.co.jp

A

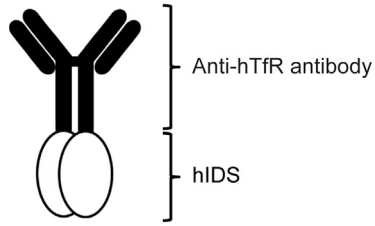

B

JR-141	k_{on} (/Ms)	k_{off} (/s)	K_D (M)
human TfR	$8.23 \pm 0.05 \times 10^{5}$	$1.01 \pm 0.03 \times 10^{-4}$	$1.22 \pm 0.04 \times 10^{-10}$
monkey TfR	$3.76 \pm 0.15 \times 10^{5}$	$3.26 \pm 0.31 \times 10^{-3}$	$8.65 \pm 0.49 \times 10^{-10}$
human M6PR	$1.51 \pm 0.00 \times 10^{5}$	$1.39 \pm 0.00 \times 10^{-3}$	$9.22 \pm 0.03 \times 10^{-9}$
naked hIDS	**k_{on} (/Ms)**	**k_{off} (/s)**	**K_D (M)**
human M6PR	$9.36 \pm 0.17 \times 10^{5}$	$3.82 \pm 0.00 \times 10^{-3}$	$4.08 \pm 0.08 \times 10^{-9}$

Figure 1. Binding Affinities of the anti-hTfR Antibody-Fused hIDS for TfRs and Human hM6PR

(A) Schematic representation of JR-141, an anti-hTfR antibody-fused hIDS used in this study. (B) Affinity of JR-141 for human and monkey TfRs and human M6PR. Affinity of naked hIDS for human M6PR is also shown (mean ± SD, n = 3). k_{on}, association rate constant; k_{off}, dissociation rate constant; K_D, equilibrium dissociation constant.

transferrin, can cross the BBB through their specific receptors expressed on the luminal side of brain capillary endothelial cells.[21–23] This BBB-penetrating system of endogenous proteins, called receptor-mediated transcytosis (RMT), may be utilized for delivery of intravenously administered proteins to the brain.[24–31] Indeed, intravenously injected humanized transferrin receptor (TfR)/β-secretase bispecific antibodies to non-human primates were shown to be distributed in the brain and to reduce amyloid-β,[32] which accumulated in the brain of patients with Alzheimer's disease.[33] For MPS II, the hIDS-fused humanized antibody against the insulin receptor (HIRMAb-IDS),[34] and the fusion protein consisting of a mouse/rat chimeric monoclonal antibody against mouse TfR and hIDS (cTfRMAb-IDS)[35] were shown to be distributed in the monkey and mouse brains, respectively. However, neither study reported a reduction in the pathological accumulation of GAGs in the brain or cerebrospinal fluid, which relate to the pathogenesis of the neurological defects observed in MPS II.[36] Therefore, there is still an unmet medical need for patients with severe forms of MPS II. In the present study, we report the development of a novel BBB-penetrating hIDS, designated JR-141. JR-141 was distributed in the brain of mice and monkeys, and reduced GAG levels in the brain of a mouse model of MPS II.

RESULTS

Preparation of JR-141 and Its Binding to hTfR and hM6PR

JR-141 is a recombinant fusion protein, produced by Chinese hamster ovary (CHO) cells, consisting of a humanized anti-hTfR antibody and hIDS. In this protein, hIDS is fused at its N terminus with the Fc domain of the antibody (Figure 1A; see the Materials and Methods for a detailed description). The affinity of JR-141 for TfR was first determined using biolayer interferometry. JR-141 exhibited a concentration-dependent binding to the extracellular domain of human and monkey TfRs with dissociation constant (K_D) values of 1.22×10^{-10} M and 8.65×10^{-10} M, respectively (Figure 1B). We confirmed that JR-141 does not bind mouse TfR. Since the target epitope in hTfR recognized by the anti-hTfR antibody used in the fusion protein was distant from the transferrin binding site, JR-141 did not interfere with the binding of transferrin to the receptor. The affinity of JR-141 for the extracellular domain 9 of human M6PR was also determined because it has been known that lysosomal proteins are transported into cells mediated by this receptor and that the domain 9 binds M6P with a high affinity.[37] The K_D value of the binding of JR-141 to human M6PR was 9.22×10^{-9} M, while that of the naked hIDS (without fusion with the anti-hTfR antibody) was 4.08×10^{-9} M (Figure 1B). We did not measure the affinity of the naked hIDS for TfR because it is assumed not to bind TfR.

Incorporation of JR-141 into Human Fibroblasts

To confirm that JR-141 undergoes receptor-mediated uptake into cells, we tested the cellular uptake of JR-141 using CCD-1076Sk normal human fibroblasts in culture. Various concentrations of JR-141 or the naked hIDS were added to the culture medium, and the intracellular concentrations of the protein were determined by electrochemiluminescent immunoassay using the anti-hIDS monoclonal antibody. As a result, JR-141 and hIDS were detected in the cells in a concentration-dependent manner (Figure 2A). In the presence of an excess amount of M6P, the uptake of JR-141 showed only a minor increase during the incubation period (Figure 2B), suggesting that the uptake into the fibroblasts was largely dependent on M6PR. The uptake was also reduced by the addition of the humanized hTfR monoclonal antibody, although the inhibition was minor (Figure 2B), probably due to low expression of TfR in CCD-1076Sk fibroblasts. These results indicate that the hTfR antibody-fused hIDS enzyme JR-141 is incorporated into the cells through hTfR as well as M6PR.

Pharmacokinetics and Brain Distribution of JR-141 in Mice

We next examined the pharmacokinetics of JR-141 in mice. Because the humanized anti-hTfR antibody that was used in JR-141 cannot react with mouse TfR, we produced mice bearing a knockin allele of the human transferrin receptor (*TFRC*) gene (*TFRC*-KI mice) (Figure S1; Supplemental Materials and Methods). When the same amount (1 mg/kg) of JR-141 or naked hIDS enzyme was intravenously administered to the knockin mice, the concentrations of

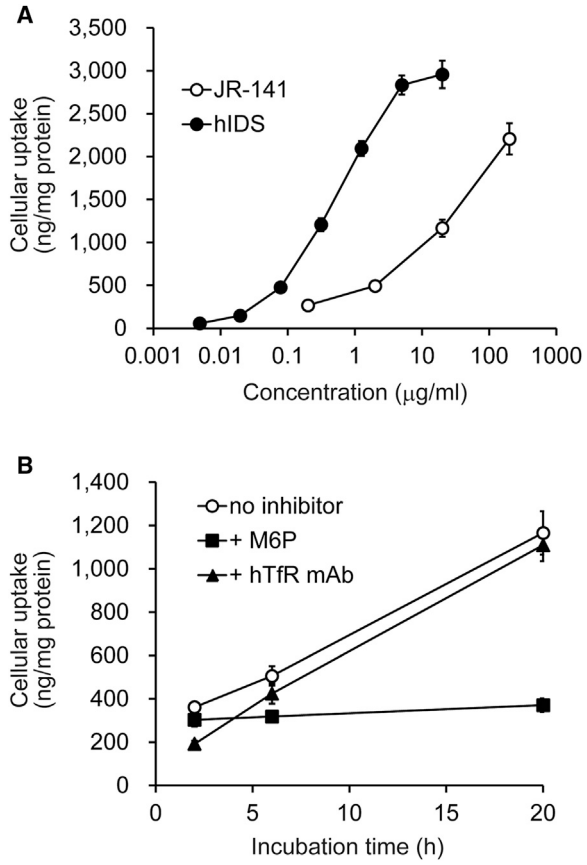

Figure 2. The Receptor-Mediated Incorporation into Fibroblasts

(A) Concentration-dependent incorporation of JR-141 or naked hIDS into CCD-1076Sk human fibroblasts determined by electrochemiluminescent immunoassay using the anti-hIDS monoclonal antibodies. The incubation time was 20 hr. The values were normalized by the amount of total cellular protein (mean ± SD, n = 3). (B) Inhibition of JR-141 incorporation by M6P (10 mM) or the humanized anti-hTfR monoclonal antibody (400 μg/mL). The concentration of the drugs used in this experiment was 20 μg/mL. The calculated molecular weights (without sugar chains) of JR-141 and naked hIDS are 265,110.93 and 59,274.99, respectively.

plasma JR-141 were higher than those of the naked enzyme (Figure 3A; Table S1). The concentrations of JR-141 in the heart, kidney, liver, lung, and spleen are shown in Figure S2. Notably, JR-141, but not the naked hIDS enzyme, was detectable in the homogenates of the brains of *TFRC*-KI mice throughout the test period (Figure 3B), and the immunoreactivity of JR-141 was found in the brain (Figures 3C and S3A). We determined the concentrations of JR-141 in the brain parenchyma and capillaries separately and confirmed that the drug was distributed in the parenchyma of the brain (Figures S3B and S3C). The concentration of JR-141 in the parenchyma increased as its level decreased in the capillaries (Figures S3B and S3C), suggesting that the drug penetrates the BBB into the brain parenchyma over time. The ratio of the concentration of JR-141 in the parenchyma and that in the capillaries was approximately 1:10. The results of *in vivo* and *ex vivo* imaging also showed the distribution of JR-141 in the brain (Figures 3D and 3E).

Pharmacokinetics and Brain Distribution of JR-141 in Monkeys

To extend the findings obtained from the mouse study to primates, we performed a pharmacokinetic study in cynomolgus monkeys (*Macaca fascicularis*). As shown in Figure 1B, JR-141 bound to monkey TfR, as well as to hTfR. When JR-141 was intravenously injected at a dose of 5 mg/kg body weight (BW) to monkeys, the half-life of JR-141 in the plasma was 4.69 hr (Figure 4A; Table S2), which was comparable to that in mice. JR-141 was also detected in the peripheral tissues, such as the heart, kidney, liver, lung, and spleen (Figure 4B). Importantly, measurable amounts of JR-141 were found in the homogenates of the cerebral cortex, cerebellum, hippocampus, and spinal cord (Figure 4C). In addition, immunohistochemistry of the brain showed that JR-141 was found in Purkinje cells in the cerebellum and pyramidal cells in the hippocampus (Figures 4D, 4E, and S4), which play important roles in motor control, cognitive function, and memory.[38] These results provide evidence that JR-141 penetrates the BBB and is distributed into the parenchyma of the brain of non-human primates.

Reduction of Brain GAG Levels by Intravenous Administration of JR-141 in MPS II Mice

Finally, to elucidate the efficacy of JR-141, we generated *TFRC*-KI mice lacking *Ids*, the gene responsible for the pathogenesis of MPS II, by crossbreeding *TFRC*-KI mice with *Ids*-knockout (KO) mice.[39] JR-141 was intravenously administered to the *TFRC*-KI/*Ids*-KO double-mutant mice at a dose of 1, 3, or 10 mg/kg once a week for 4 weeks, and the concentrations of GAGs in the peripheral tissues tested and in the brain were measured. Both JR-141 and the naked hIDS enzyme reduced GAG levels in peripheral tissues including the heart, kidney, liver, lung, and spleen, and the efficacy in these tissues by the hIDS at 0.5 mg/kg was similar to that of JR-141 at 1 or 3 mg/kg (Figure 5; Table S3). This may reflect the fact that 1 mg of JR-141 contains a similar mol amount of IDS enzyme to 0.5 mg of the naked hIDS. Although the naked hIDS (0.5 mg/kg) failed to decrease GAGs in the brain, JR-141 at a dose of 1 mg/kg partially, but significantly, suppressed the accumulation of GAGs in the brain. JR-141 at a dose of 3 mg/kg reduced the GAG level in the brain of *TRFC*-KI/*Ids*-KO mice to a level found in wild-type (WT) mice (Figure 5; Table S3). Our data suggest that JR-141 normalizes the metabolism of GAGs in both the brain and the peripheral tissues of the mouse model of MPS II.

DISCUSSION

We developed a novel BBB-penetrating enzyme, JR-141, for the treatment of patients with MPS II with CNS disorders and showed that JR-141 crossed the BBB into the brain parenchyma of both mice and monkeys. Intravenously injected JR-141 reduced the accumulation of GAGs in the brain of MPS II model mice.

Impairment of metabolism of heparan sulfate, a major type of sulfated GAGs, leads to the accumulation of gangliosides, resulting in neurological defects, possibly through multiple mechanisms, including hyperphosphorylation of tau protein, endoplasmic reticulum stress, and increased autophagy.[40–42] Normalization of GAG metabolism

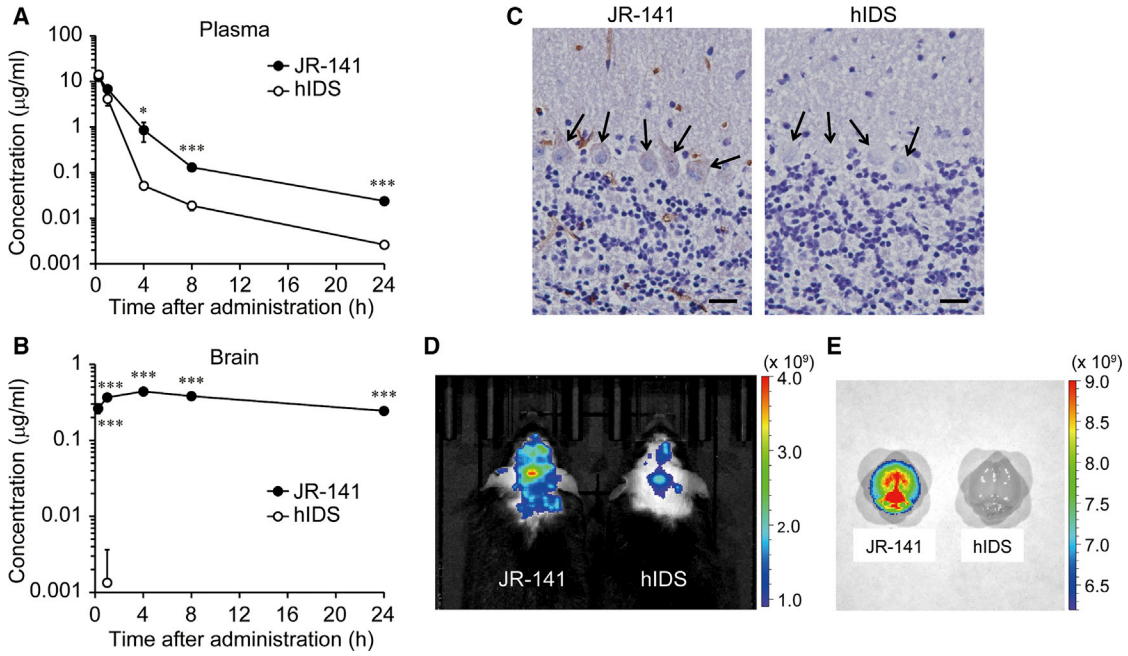

Figure 3. Distribution of JR-141 in *TFRC*-KI Mice after Intravenous Administration

(A and B) Pharmacokinetics of JR-141 and naked hIDS in the plasma (A) and the brain homogenates (B). Either JR-141 or the naked enzyme was intravenously administered at a dose of 1 mg/kg. The concentrations of these recombinant proteins were determined by electrochemiluminescent immunoassay (mean ± SD, n = 3; *p < 0.05, ***p < 0.001, t test). Concentrations of the naked hIDS in the brain were incidentally detected at low level in only one animal 1 hr after administration. Statistical analysis was performed using the lower limit value of detection for other animals and other time points. See Table S1 for detailed pharmacokinetic parameters with moment analysis and Figure S2 for distribution of JR-141 and hIDS in peripheral tissues. (C) Immunohistochemical analysis in the brain of *TFRC*-KI mice 24 hr after intravenous injection of JR-141 or naked hIDS. Arrows indicate Purkinje cells. Scale bars, 20 μm. (D) *In vivo* imaging of the mice using IVIS Lumina III. Images were acquired at 24 hr after intravenous injection of JR-141 or hIDS. (E) *Ex vivo* imaging of resected brains after saline perfusion. Color bars indicate radiant efficiency ([p/s/cm^2/sr]/[mW/cm^2]).

in the brain is likely to prevent the development or progression of CNS symptoms. Indeed, direct (i.e., intraventricular or intrathecal) administration of hIDS to the brain of model animals reduced the storage of GAGs and improved neurological function.[39,43,44]

Recently, a clinical study has been conducted for direct delivery of hIDS to the brain,[45] in which cognitively impaired patients with MPS II were treated with recombinant hIDS via an indwelling intrathecal drug delivery device. In that study, although the concentration of GAGs in the cerebrospinal fluid was reported to be reduced by 80%–90%, depending on the dose, after 6 months, 75% of patients experienced adverse events related to the device.[45] Therefore, the use of direct delivery of the drug to the brain is limited in clinical settings due to its invasiveness and safety concerns. Moreover, the patients were required to continue intravenous hIDS injection as well for the treatment of peripheral defects even after the intrathecal administration of hIDS.[45]

In general, one of the obstacles in the evaluation of the feasibility of antibody-based recombinant proteins for clinical use is that humanized antibodies often have lower affinity against their target molecules in the test animals than in humans. Since JR-141 is not recognized by mouse TfR, we cannot examine the efficacy of this protein in WT mice. The anti-mouse TfR antibody fusion enzyme could be used as a surrogate molecule for JR-141. Indeed, anti-mouse TfR antibody-fused hIDS (cTfRMAb-IDS) has been reported to be distributed in the brain and spinal cord.[35] However, the properties of the surrogate molecule are not identical to those of the real drug candidate. We have overcome this obstacle by establishing and utilizing *TFRC*-KI/*Ids*-KO mice, in which the mouse *Tfrc* gene is replaced with the human *TFRC* gene and the *Ids* gene is lacking. So far, there is no other humanized anti-hTfR antibody-fused hIDS recombinant protein that inhibits the accumulation of GAGs in the brain of MPS II model animals.

Besides TfR, the insulin receptor represents another potential target for BBB-penetrating drug technology. In fact, anti-human insulin receptor antibody-fused enzymes including α-L-iduronidase (HIRMAb-IDUA),[46,47] IDS,[34] N-sulfoglucosamine sulfohydorase,[48] and α-N-acetylglucosaminidase[49] have been under development for the treatment of MPS I (Hurler syndrome), MPS II, MPS IIIA, and IIIB (Sanfilippo syndromes A and B), respectively. These drugs may have agonistic or antagonistic effects on the human insulin receptor, which raises concern regarding perturbation of glycemic control in the patients, though a non-clinical study in monkeys showed that chronic treatment of HIRMAb-IDUA did not affect glucose tolerance.[47]

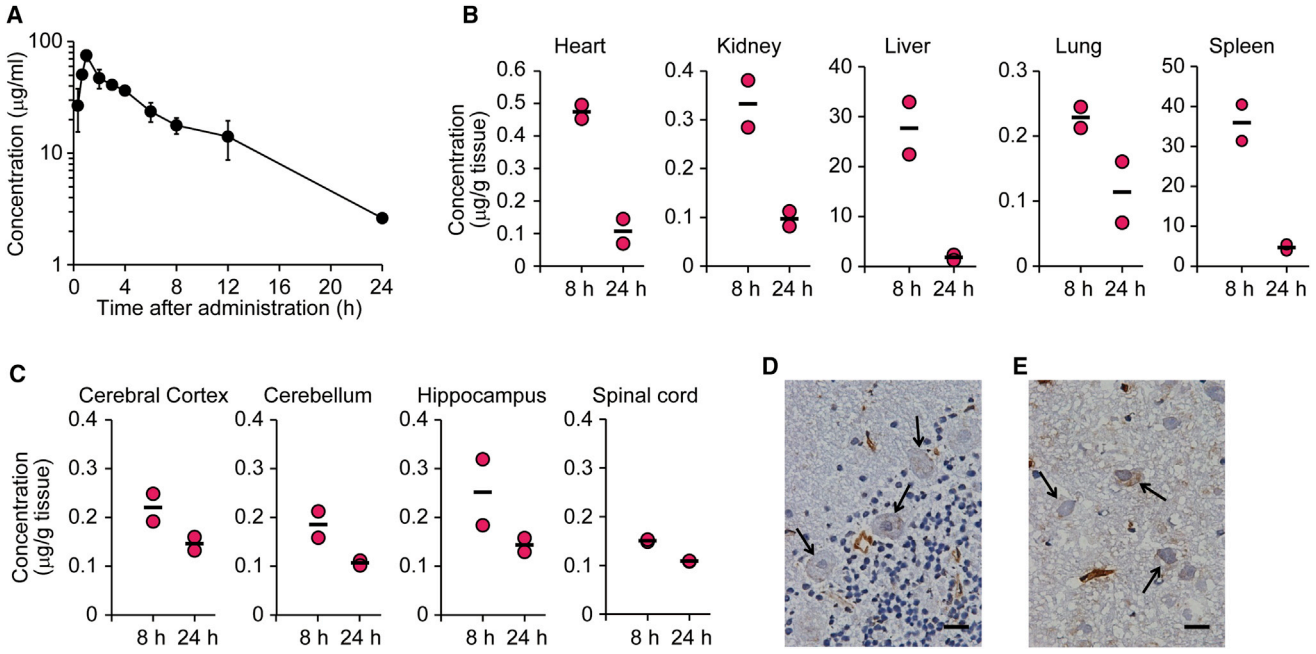

Figure 4. Distribution of JR-141 in Cynomolgus Monkeys after Intravenous Administration

(A) Pharmacokinetics of JR-141 in the plasma of the monkey. JR-141 was administered intravenously at a dose of 5 mg/kg (0–8 hr, n = 4; 12 and 24 hr, n = 2). Data were plotted as mean ± SD. Detailed pharmacokinetic parameters are presented in Table S2. (B and C) Concentrations of JR-141 in the peripheral tissues (B) and the brain and spinal cord (C). The heart, kidney, liver, lung, spleen, cerebral cortex, cerebellum, hippocampus, and spinal cord were resected. JR-141 in each tissue homogenate was quantified by electrochemiluminescent immunoassay (n = 2). Bars indicate the mean. (D) Immunohistochemical analysis of the cerebellum. Arrows indicate Purkinje cells. (E) Immunohistochemical analysis of the hippocampus. Arrows indicate the pyramidal cells. The brains were resected at 8 hr after the administration. Scale bars, 20 μm.

Based on the present results, we reason that JR-141 crosses the BBB by utilizing RMT of transferrin and is distributed to the parenchyma of the brain, although the exact mechanism of the delivery remains to be elucidated. In addition, we need to confirm the efficacy of JR-141 on neurological functions, such as learning and memory, in MPS II model animals in a future study. Nevertheless, the present findings provide a proof of concept for translation of JR-141 to clinical study and show the feasibility of the use of JR-141 as a convenient and minimally invasive therapy for patients with MPS II with CNS manifestations. A phase I/II clinical trial of JR-141 for MPS II is currently underway. The anti-hTfR antibody-based strategy for delivery of drugs into the brain could be applicable to other neurologic diseases, provided that the antibody has appropriate binding properties for hTfR.

MATERIALS AND METHODS

Antibodies

A horseradish peroxidase (HRP)-conjugated monkey adsorbed anti-human immunoglobulin G (IgG) antibody was purchased from Bethyl Laboratories (A80-319P, Montgomery, TX). An anti-hIDS polyclonal antibody raised in rabbits against recombinant hIDS, and an anti-hTfR monoclonal antibody raised in mice against the extracellular domain of hTfR were produced in house. Two different clones of anti-hIDS monoclonal antibodies used for the electrochemiluminescence assay were raised in mice against recombinant hIDS. One clone was a conjugate with SULFO-TAG using MSD GOLD SULFO-TAG NHS-Ester (Meso Scale Diagnostics, Gaithersburg, MD), and the other clone was labeled with biotin by NHS-PEO_4-Biotin (Pierce, Rockford, IL).

Animals

All animal experiments were performed with the approval of the Institutional Animal Care and Use Committees of JCR Pharmaceuticals and Shin Nippon Biomedical Laboratories (Kagoshima, Japan). The establishment of *Ids*-KO mice in a C57BL/6 background was described previously.[39] The mice exhibit symptoms similar to those of patients with MPS II,[39] which warrants their use as a model of MPS II. The generation of *TFRC*-KI mice is described in Figure S1 and the Supplemental Materials and Methods. To obtain *TFRC*-KI/*Ids*-KO double-mutant mice, *Ids*-KO mice were crossbred with *TFRC*-KI mice. C57BL/6 mice were purchased from Charles River Japan (Yokohama, Japan). Monkey experiments were performed in Shin Nippon Biomedical Laboratories.

Preparation of the Humanized anti-hTfR Antibody-Fused hIDS Protein (JR-141)

JR-141 is a recombinant fusion protein resulting from the binding of hIDS to a humanized anti-human TfR antibody with the IgG1 subclass and is a hetero-tetramer glycoprotein. The antibody moiety comprises the complementarity-determining region of a mouse

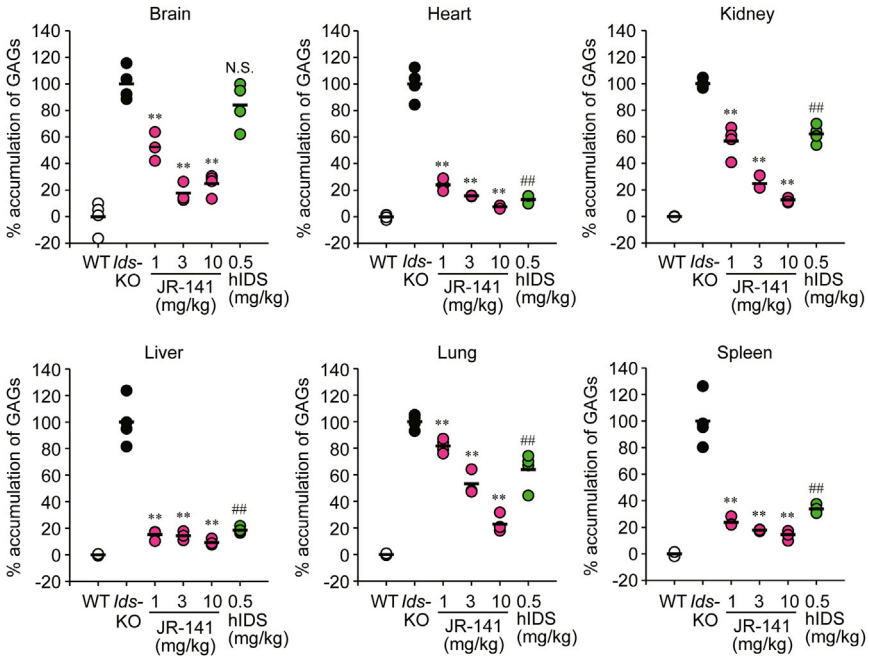

Figure 5. Reduction in Accumulation of GAGs by JR-141 in the Brain and the Peripheral Tissues of *TFRC*-KI/*Ids*-KO Double-Mutant Mice

JR-141 was intravenously administered to the mice at a dose of 1, 3, or 10 mg/kg BW once a week for 4 weeks. GAGs were quantified 1 week after the final dosing in the resected brain, heart, kidney, liver, lung, and spleen. Values are expressed as % accumulation when mean GAG levels in the WT mice were considered to be 0% and those in *Ids*-KO mice were considered to be 100%. Bars indicate the mean for each group (n = 4). $^{**}p < 0.01$ by Dunnett test (*Ids*-KO versus JR-141 groups) and $^{\#\#}p < 0.01$ by Student's t test (*Ids*-KO versus hIDS groups). N.S., not significant. The absolute values of the concentration and detailed statistical analysis between groups are presented in Table S3.

anti-human TfR monoclonal antibody, a variable region consisting of the human γ1 chain or κ chain framework region and their constant regions. One N-binding sugar chain is present in the Fc region of the antibody. The enzyme moiety is hIDS, having eight N-binding sugar chains (Figure S5). The calculated molecular weight of JR-141 is 265,110.93. The fusion protein was produced by introducing into CHO cells a cDNA consisting of hIDS and humanized anti-human TfR antibody. The CHO cells were cultured with a serum-free medium, and proteins released into the culture medium were collected and subjected to virus inactivation, followed by a multi-step chromatographic purification and virus removal. The homogeneity was determined by SDS-PAGE and size-exclusion high-performance liquid chromatography.[50] The naked hIDS enzyme was also produced by CHO cells. Enzyme activity of JR-141 and the naked enzyme were determined using 4-methylumbelliferyl-sulfate (Sigma-Aldrich, St. Louis, MI) as a substrate. These recombinant proteins were stored in sterile vials at −80°C until use.

Affinity of JR-141 against TfR and M6PR

Affinity between JR-141 and TfR was determined with Bio-Layer Interferometry using the Octet RED96 system (Pall ForteBio, Fremont, CA). Various concentrations of JR-141 in HBS-P+ buffer (10 mM 2-[4-(2-hydroxyethyl)-1-piperazinyl]ethanesulfonic acid [HEPES], 150 mM NaCl, 50 μM EDTA, and 0.05% Surfactant P20) containing 1% BSA were added into a 96-well black microplate at a volume of 200 μL/well. Wells for baseline and dissociation measurements, as well as regeneration buffer (10 mM glycine-HCl [pH 1.7])-containing wells were also prepared. The plate was agitated at 1,000 rpm throughout the measurement. The recombinant proteins of the extracellular domain of TfR of human and cynomolgus monkey with N-terminal 6× His tag were immobilized onto a nitrilotriacetic acid (NTA) biosensor (threshold, 1.0) at the loading step. The association and dissociation periods were set at 120 s and 200–300 s, respectively. Kinetic constants were calculated from the sensorgram using the 1:1 (Langmuir) binding model of Octet Data Analysis Software.

Affinity between JR-141 and M6PR was determined with the surface plasmon resonance method using the Biacore T200 system. The recombinant protein of the domain 9 of human cation-independent M6PR fused with C-terminal 6× His tag (MPRdom9-His) was immobilized onto a Ni-NTA sensor chip at a low density (~300 resonance units [RU]). Various concentrations of JR-141 in HBS-P+ were injected at 50 μL/min. Measurement was performed using the Single Cycle Kinetics mode (association time, 300 s; dissociation time, 180 s). Sensor surface was regenerated with the regeneration buffer (10 mM HEPES, 150 mM NaCl, 350 mM EDTA, and 0.05% Surfactant P20). Kinetic constants were calculated from the sensorgram using the 1:1 (Langmuir) binding model of Biacore T200 Evaluation Software v3.0.

Incorporation of JR-141 into Human Fibroblast Cells

CCD-1076Sk normal human fibroblasts (DS Pharma Biomedical, Osaka, Japan) were seeded onto 96-well plates at a density of 2.0×10^4 cells/well and cultured for 3 days. Various concentrations of JR-141 were added to the culture medium and incubated at 37°C for 20 hr. The cells were lysed with M-PER (Pierce) containing 0.5% Protease Inhibitor Cocktail (Sigma-Aldrich) after being washed with ice-cold PBS, and the extracts were mixed with the biotin-labeled anti-hIDS monoclonal antibody and another clone of the SULFO-TAG-labeled anti-hIDS monoclonal antibody. The reaction mixtures were then added to a streptavidin-coated plate, and the intensity of electrochemiluminescence was quantified by Sector Imager 6000 (Meso Scale Diagnostics, Rockville, MD). The values were normalized by the total cellular protein content determined by the bicinchoninic

acid protein assay method. Inhibition of receptor-mediated uptake was examined in the presence of 10 mM M6P or 400 μg/mL humanized anti-hTfR monoclonal antibody.

Pharmacokinetics in *TFRC*-KI Mice

JR-141 or naked hIDS enzyme was administered to *TFRC*-KI male mice (12–24 weeks of age) at a dose of 1 mg/kg BW. Blood samples were collected under isoflurane anesthesia from the left ventricle of each mouse at 15 min and at 1, 4, 8, and 24 hr after dosing, and the plasma was obtained by centrifugation with EDTA-2K (n = 3 at each time point). After the blood samples were collected at each time point, mice were perfused with physiological saline via the left ventricle, and then the brain, heart, liver, kidney, lung, and spleen were removed. The resected tissues were homogenized using a bead beater-type homogenizer in a buffer containing the Protease Inhibitor Cocktail and subjected to centrifugation to obtain the tissue lysate as a supernatant. JR-141 was quantified with a validated in-house electrochemiluminescent assay system (Figure S6). In brief, the samples were mixed with the biotin-labeled anti-human IgG light-chain antibody (for plasma JR-141) or the biotin-labeled anti-hIDS monoclonal antibody (for the naked hIDS and tissue JR-141) and another clone of the SULFO-TAG-labeled anti-hIDS monoclonal antibody and incubated at room temperature for 1 hr. Subsequently, the reactions were added to a pre-blocked streptavidin-coated plate, settled for 1 hr, and the intensity of electrochemiluminescence was quantified by Sector Imager 6000 (Meso Scale Diagnostics). Pharmacokinetic parameters were calculated with moment analysis.

Immunohistochemistry in *TFRC*-KI Mouse Brain

The resected brain was embedded in optimum cutting temperature (OCT) compound, and 4-μm frozen sections were obtained. The sections were fixed with 4% paraformaldehyde, blocked with SuperBlock (PBS) blocking buffer for 1 hr, and reacted with the anti-hIDS antibody for 4 hr, and then with CSA II Rabbit Link for 15 min. The sections were reacted with the TSA Plus Fluorescein System (Perkin Elmer, Waltham, MA) for 15 min. Subsequently, the specimens were incubated with the HRP-conjugated anti-fluorescein antibody for 15 min and visualized with 3,3′-diaminobenzidine. Counter staining was performed with hematoxylin.

To estimate the ratio of the concentration of JR-141 in the parenchyma and that in the capillary, the brain was gently homogenized in Hank's balanced salt solution containing 18% dextran with a protease inhibitor cocktail (Sigma-Aldrich) using a glass homogenizer, and the homogenates were centrifuged at 5,400 × *g* for 15 min. The supernatant containing the brain parenchymal lysate was removed from the pellet and subjected to quantification of JR-141. The pellet containing the brain capillary was solubilized with a RIPA buffer (Wako Pure Chemical, Osaka, Japan). The concentration of JR-141 was determined as described above.

In Vivo and *Ex Vivo* Imaging Using IVIS

XenoLight CF750 (Caliper, Arcade, NY) labeling was carried out according to the manufacturer's instructions. In order to equalize protein concentrations and fluorescent intensities between JR-141 and naked hIDS, labeled and unlabeled test substances were properly mixed. These test substances (5 mg/kg) were administered intravenously to *TFRC*-KI mice. Whole-body (*in vivo*) fluorescent images were captured with IVIS Lumina III (Perkin Elmer) before dosing, and at 24 hr after dosing, under anesthesia. Mice were then perfused with physiological saline, and the brains were resected and subjected to *ex vivo* imaging.

Monkey Studies

To study the pharmacokinetics in monkeys, JR-141 was administered intravenously to male cynomolgus monkeys (2–3 years of age) at a dose of 5 mg/kg BW. The blood samples were obtained at 20 min, and at 1, 2, 3, 4, 6, 8, 12, and 24 hr after administration (0–8 hr, n = 4; 12 and 24 hr, n = 2). At 8 and 24 hr after dosing, whole-body perfusion was performed in monkeys that received 5 mg/kg of the drug with physiological saline, and the brain, spinal cord, heart, kidney, liver, lung, and spleen were resected. The concentration of JR-141 in each tissue was determined by the method used in the mouse study.

For immunohistochemical analysis, the brains were resected at 8 hr after drug administration and embedded in OCT compound, and 4-μm frozen sections were obtained. The sections were fixed with 4% paraformaldehyde, and immersed in 0.3% H_2O_2/methanol solution to inactivate endogenous peroxidase activity, blocked with skim milk containing 0.05% Tween 20 for 2 hr, and reacted with the monkey adsorbed HRP-labeled human IgG antibody (Bethyl) for 2 hr and then with Amplification Reagent of the CSA II biotin-free tyramide signal amplification system (Dako) for 30 min. Subsequently, the specimens were incubated with the HRP-conjugated anti-fluorescein antibody for 15 min and visualized with 3,3′-diaminobenzidine. Counter staining was performed with hematoxylin.

Measurement of GAGs in *TFRC*-KI/*Ids*-KO Mice

JR-141 was intravenously administered to the *TFRC*-KI/*Ids*-KO double-mutant mice (male, 18–32 weeks of age) at a dose of 1, 3, or 10 mg/kg BW once a week for 4 weeks (n = 3–4). One week after the final dosing, tissues were resected and lyophilized. Small pieces of the lyophilized tissues cut with scissors were suspended in 0.5 M Tris-HCl buffer (pH 7.5) and digested with actinase E (Kaken Pharmaceuticals, Osaka, Japan) at 60°C for 16 hr. The digests were centrifuged, and the supernatants were collected. The concentration of sulfated GAGs in the tissue extracts was determined with the Wieslab sGAG quantitative kit (Euro Diagnostica, Arnhem, the Netherlands), according to the manufacturer's instructions.

Statistics

Data are expressed as means and SDs. The statistical analysis was conducted with the SPSS Statistics software (IBM, Armonk, NY). Student's t test was used to compare differences between two groups, and Dunnett's test was used to compare differences among three or more groups. p values < 0.05 were considered to indicate

statistical significance. No statistical method was employed for immunohistochemistry.

SUPPLEMENTAL INFORMATION

Supplemental Information includes Supplemental Materials and Methods, six figures, and three tables and can be found with this article online at https://doi.org/10.1016/j.ymthe.2018.02.032.

AUTHOR CONTRIBUTIONS

H.S. and K. Takahashi designed and supervised the study, performed the experiments, and analyzed the data. R.Y., K. Tachibana, and T.H. designed and supervised the study and analyzed the data. H.M., E.Y., Y.K., M.K., G.G., and H.T. performed the experiments and analyzed the data. A.M. supervised and performed histochemical experiments. K.M. analyzed the data and wrote the manuscript. H.S., H.M., E.Y., M.K., R.Y., T.H., and K. Takahashi edited the manuscript. All authors read and approved the manuscript.

CONFLICTS OF INTEREST

H.M., H.S., E.Y., Y.K., M.K., G.G., H.T., R.Y., K.M., K. Tachibana, T.H., and K. Takahashi receive compensation as employees of JCR Pharmaceuticals.

ACKNOWLEDGMENTS

We thank Yoshimi Takai (Kobe University) for helpful discussions and suggestions for this study. We also thank him and Kiyohito Mizutani (Kobe University) for critical reading of this manuscript.

REFERENCES

1. Schultz, M.L., Tecedor, L., Chang, M., and Davidson, B.L. (2011). Clarifying lysosomal storage diseases. Trends Neurosci. *34*, 401–410.
2. Tylki-Szymańska, A. (2014). Mucopolysaccharidosis type II, Hunter's syndrome. Pediatr. Endocrinol. Rev. *12* (*Suppl 1*), 107–113.
3. Wilson, P.J., Morris, C.P., Anson, D.S., Occhiodoro, T., Bielicki, J., Clements, P.R., and Hopwood, J.J. (1990). Hunter syndrome: isolation of an iduronate-2-sulfatase cDNA clone and analysis of patient DNA. Proc. Natl. Acad. Sci. USA *87*, 8531–8535.
4. Neufeld, E.F., and Muenzer, J. (2001). The mucopolysaccharidoses. In The Metabolic & Molecular Bases of Inherited Disease, C.R. Scriver, A.L. Beaudet, W.S. Sly, and D. Valle, eds. (McGraw Hill), pp. 3421–3452.
5. Al Sawaf, S., Mayatepek, E., and Hoffmann, B. (2008). Neurological findings in Hunter disease: pathology and possible therapeutic effects reviewed. J. Inherit. Metab. Dis. *31*, 473–480.
6. Malm, G., Lund, A.M., Månsson, J.E., and Heiberg, A. (2008). Mucopolysaccharidoses in the Scandinavian countries: incidence and prevalence. Acta Paediatr. *97*, 1577–1581.
7. Nelson, J., Crowhurst, J., Carey, B., and Greed, L. (2003). Incidence of the mucopolysaccharidoses in Western Australia. Am. J. Med. Genet. A. *123A*, 310–313.
8. Khan, S.A., Peracha, H., Ballhausen, D., Wiesbauer, A., Rohrbach, M., Gautschi, M., Mason, R.W., Giugliani, R., Suzuki, Y., Orii, K.E., et al. (2017). Epidemiology of mucopolysaccharidoses. Mol. Genet. Metab. *121*, 227–240.
9. Baehner, F., Schmiedeskamp, C., Krummenauer, F., Miebach, E., Bajbouj, M., Whybra, C., Kohlschütter, A., Kampmann, C., and Beck, M. (2005). Cumulative incidence rates of the mucopolysaccharidoses in Germany. J. Inherit. Metab. Dis. *28*, 1011–1017.
10. Nelson, J. (1997). Incidence of the mucopolysaccharidoses in Northern Ireland. Hum. Genet. *101*, 355–358.
11. Lin, H.Y., Lin, S.P., Chuang, C.K., Niu, D.M., Chen, M.R., Tsai, F.J., Chao, M.C., Chiu, P.C., Lin, S.J., Tsai, L.P., et al. (2009). Incidence of the mucopolysaccharidoses in Taiwan, 1984-2004. Am. J. Med. Genet. A. *149A*, 960–964.
12. Ohashi, T. (2012). Enzyme replacement therapy for lysosomal storage diseases. Pediatr. Endocrinol. Rev. *10* (*Suppl 1*), 26–34.
13. Gary-Bobo, M., Nirdé, P., Jeanjean, A., Morère, A., and Garcia, M. (2007). Mannose 6-phosphate receptor targeting and its applications in human diseases. Curr. Med. Chem. *14*, 2945–2953.
14. Muenzer, J., Beck, M., Giugliani, R., Suzuki, Y., Tylki-Szymanska, A., Valayannopoulos, V., Vellodi, A., and Wraith, J.E. (2011). Idursulfase treatment of Hunter syndrome in children younger than 6 years: results from the Hunter Outcome Survey. Genet. Med. *13*, 102–109.
15. Muenzer, J., Beck, M., Eng, C.M., Giugliani, R., Harmatz, P., Martin, R., Ramaswami, U., Vellodi, A., Wraith, J.E., Cleary, M., et al. (2011). Long-term, open-labeled extension study of idursulfase in the treatment of Hunter syndrome. Genet. Med. *13*, 95–101.
16. Okuyama, T., Tanaka, A., Suzuki, Y., Ida, H., Tanaka, T., Cox, G.F., Eto, Y., and Orii, T. (2010). Japan Elaprase Treatment (JET) study: idursulfase enzyme replacement therapy in adult patients with attenuated Hunter syndrome (Mucopolysaccharidosis II, MPS II). Mol. Genet. Metab. *99*, 18–25.
17. Giugliani, R., Hwu, W.L., Tylki-Szymanska, A., Whiteman, D.A., and Pano, A. (2014). A multicenter, open-label study evaluating safety and clinical outcomes in children (1.4-7.5 years) with Hunter syndrome receiving idursulfase enzyme replacement therapy. Genet. Med. *16*, 435–441.
18. Sohn, Y.B., Cho, S.Y., Park, S.W., Kim, S.J., Ko, A.R., Kwon, E.K., Han, S.J., and Jin, D.K. (2013). Phase I/II clinical trial of enzyme replacement therapy with idursulfase beta in patients with mucopolysaccharidosis II (Hunter syndrome). Orphanet J. Rare Dis. *8*, 42.
19. Wraith, J.E., Scarpa, M., Beck, M., Bodamer, O.A., De Meirleir, L., Guffon, N., Meldgaard Lund, A., Malm, G., Van der Ploeg, A.T., and Zeman, J. (2008). Mucopolysaccharidosis type II (Hunter syndrome): a clinical review and recommendations for treatment in the era of enzyme replacement therapy. Eur. J. Pediatr. *167*, 267–277.
20. Rubin, L.L., and Staddon, J.M. (1999). The cell biology of the blood-brain barrier. Annu. Rev. Neurosci. *22*, 11–28.
21. Pardridge, W.M., Eisenberg, J., and Yang, J. (1985). Human blood-brain barrier insulin receptor. J. Neurochem. *44*, 1771–1778.
22. Golden, P.L., Maccagnan, T.J., and Pardridge, W.M. (1997). Human blood-brain barrier leptin receptor. Binding and endocytosis in isolated human brain microvessels. J. Clin. Invest. *99*, 14–18.
23. Fishman, J.B., Rubin, J.B., Handrahan, J.V., Connor, J.R., and Fine, R.E. (1987). Receptor-mediated transcytosis of transferrin across the blood-brain barrier. J. Neurosci. Res. *18*, 299–304.
24. Jefferies, W.A., Brandon, M.R., Hunt, S.V., Williams, A.F., Gatter, K.C., and Mason, D.Y. (1984). Transferrin receptor on endothelium of brain capillaries. Nature *312*, 162–163.
25. Pardridge, W.M. (1986). Receptor-mediated peptide transport through the blood-brain barrier. Endocr. Rev. *7*, 314–330.
26. Pardridge, W.M., Eisenberg, J., and Yang, J. (1987). Human blood-brain barrier transferrin receptor. Metabolism *36*, 892–895.
27. Pardridge, W.M., Kang, Y.S., Buciak, J.L., and Yang, J. (1995). Human insulin receptor monoclonal antibody undergoes high affinity binding to human brain capillaries in vitro and rapid transcytosis through the blood-brain barrier in vivo in the primate. Pharm. Res. *12*, 807–816.
28. Osborn, M.J., McElmurry, R.T., Peacock, B., Tolar, J., and Blazar, B.R. (2008). Targeting of the CNS in MPS-IH using a nonviral transferrin-alpha-L-iduronidase fusion gene product. Mol. Ther. *16*, 1459–1466.
29. Pardridge, W.M. (2015). Blood-brain barrier drug delivery of IgG fusion proteins with a transferrin receptor monoclonal antibody. Expert Opin. Drug Deliv. *12*, 207–222.
30. Bickel, U., Yoshikawa, T., and Pardridge, W.M. (2001). Delivery of peptides and proteins through the blood-brain barrier. Adv. Drug Deliv. Rev. *46*, 247–279.

31. Yu, Y.J., and Watts, R.J. (2013). Developing therapeutic antibodies for neurodegenerative disease. Neurotherapeutics *10*, 459–472.

32. Yu, Y.J., Atwal, J.K., Zhang, Y., Tong, R.K., Wildsmith, K.R., Tan, C., Bien-Ly, N., Hersom, M., Maloney, J.A., Meilandt, W.J., et al. (2014). Therapeutic bispecific antibodies cross the blood-brain barrier in nonhuman primates. Sci. Transl. Med. *6*, 261ra154.

33. Regland, B., and Gottfries, C.G. (1992). The role of amyloid beta-protein in Alzheimer's disease. Lancet *340*, 467–469.

34. Boado, R.J., Ka-Wai Hui, E., Zhiqiang Lu, J., and Pardridge, W.M. (2014). Insulin receptor antibody-iduronate 2-sulfatase fusion protein: pharmacokinetics, anti-drug antibody, and safety pharmacology in Rhesus monkeys. Biotechnol. Bioeng. *111*, 2317–2325.

35. Zhou, Q.H., Boado, R.J., Lu, J.Z., Hui, E.K., and Pardridge, W.M. (2012). Brain-penetrating IgG-iduronate 2-sulfatase fusion protein for the mouse. Drug Metab. Dispos. *40*, 329–335.

36. Hendriksz, C.J., Muenzer, J., Vanderver, A., Davis, J.M., Burton, B.K., Mendelsohn, N.J., Wang, N., Pan, L., Pano, A., and Barbier, A.J. (2015). Levels of glycosaminoglycans in the cerebrospinal fluid of healthy young adults, surrogate-normal children, and Hunter syndrome patients with and without cognitive impairment. Mol. Genet. Metab. Rep. *5*, 103–106.

37. Hancock, M.K., Yammani, R.D., and Dahms, N.M. (2002). Localization of the carbohydrate recognition sites of the insulin-like growth factor II/mannose 6-phosphate receptor to domains 3 and 9 of the extracytoplasmic region. J. Biol. Chem. *277*, 47205–47212.

38. Pandya, D.N., and Yeterian, E.H. (1985). Architectural connections of cortical association areas. In Cerebral Cortex, *Volume 4*, A. Peters and E.G. Jones, eds. (Plenum Press), pp. 3–61.

39. Higuchi, T., Shimizu, H., Fukuda, T., Kawagoe, S., Matsumoto, J., Shimada, Y., Kobayashi, H., Ida, H., Ohashi, T., Morimoto, H., et al. (2012). Enzyme replacement therapy (ERT) procedure for mucopolysaccharidosis type II (MPS II) by intraventricular administration (IVA) in murine MPS II. Mol. Genet. Metab. *107*, 122–128.

40. Walkley, S.U., Siegel, D.A., and Dobrenis, K. (1995). GM2 ganglioside and pyramidal neuron dendritogenesis. Neurochem. Res. *20*, 1287–1299.

41. Takamura, A., Higaki, K., Kajimaki, K., Otsuka, S., Ninomiya, H., Matsuda, J., Ohno, K., Suzuki, Y., and Nanba, E. (2008). Enhanced autophagy and mitochondrial aberrations in murine G(M1)-gangliosidosis. Biochem. Biophys. Res. Commun. *367*, 616–622.

42. Ohmi, K., Kudo, L.C., Ryazantsev, S., Zhao, H.Z., Karsten, S.L., and Neufeld, E.F. (2009). Sanfilippo syndrome type B, a lysosomal storage disease, is also a tauopathy. Proc. Natl. Acad. Sci. USA *106*, 8332–8337.

43. Sohn, Y.B., Lee, J., Cho, S.Y., Kim, S.J., Ko, A.R., Nam, M.H., and Jin, D.K. (2013). Improvement of CNS defects via continuous intrathecal enzyme replacement by osmotic pump in mucopolysaccharidosis type II mice. Am. J. Med. Genet. A. *161A*, 1036–1043.

44. Calias, P., Papisov, M., Pan, J., Savioli, N., Belov, V., Huang, Y., Lotterhand, J., Alessandrini, M., Liu, N., Fischman, A.J., et al. (2012). CNS penetration of intrathecal-lumbar idursulfase in the monkey, dog and mouse: implications for neurological outcomes of lysosomal storage disorder. PLoS ONE *7*, e30341.

45. Muenzer, J., Hendriksz, C.J., Fan, Z., Vijayaraghavan, S., Perry, V., Santra, S., Solanki, G.A., Mascelli, M.A., Pan, L., Wang, N., et al. (2016). A phase I/II study of intrathecal idursulfase-IT in children with severe mucopolysaccharidosis II. Genet. Med. *18*, 73–81.

46. Boado, R.J., Hui, E.K., Lu, J.Z., and Pardridge, W.M. (2009). AGT-181: expression in CHO cells and pharmacokinetics, safety, and plasma iduronidase enzyme activity in Rhesus monkeys. J. Biotechnol. *144*, 135–141.

47. Boado, R.J., Hui, E.K., Lu, J.Z., and Pardridge, W.M. (2012). Glycemic control and chronic dosing of rhesus monkeys with a fusion protein of iduronidase and a monoclonal antibody against the human insulin receptor. Drug Metab. Dispos. *40*, 2021–2025.

48. Boado, R.J., Lu, J.Z., Hui, E.K., and Pardridge, W.M. (2014). Insulin receptor antibody-sulfamidase fusion protein penetrates the primate blood-brain barrier and reduces glycosoaminoglycans in Sanfilippo type A cells. Mol. Pharm. *11*, 2928–2934.

49. Boado, R.J., Lu, J.Z., Hui, E.K., Lin, H., and Pardridge, W.M. (2016). Insulin receptor antibody-α-N-acetylglucosaminidase fusion protein penetrates the primate blood-brain barrier and reduces glycosoaminoglycans in Sanfilippo type B fibroblasts. Mol. Pharm. *13*, 1385–1392.

50. Sonoda, H., and Takahashi, K. (2016) Anti-human transferrin receptor antibody permeating blood-brain barrier. International patent WO 2016/208695 A1, filed June 24, 2016, and published December 29, 2016.

YMTHE, Volume *26*

Supplemental Information

A Blood-Brain-Barrier-Penetrating Anti-human Transferrin Receptor Antibody Fusion Protein for Neuronopathic Mucopolysaccharidosis II

Hiroyuki Sonoda, Hideto Morimoto, Eiji Yoden, Yuri Koshimura, Masafumi Kinoshita, Galina Golovina, Haruna Takagi, Ryuji Yamamoto, Kohtaro Minami, Akira Mizoguchi, Katsuhiko Tachibana, Tohru Hirato, and Kenichi Takahashi

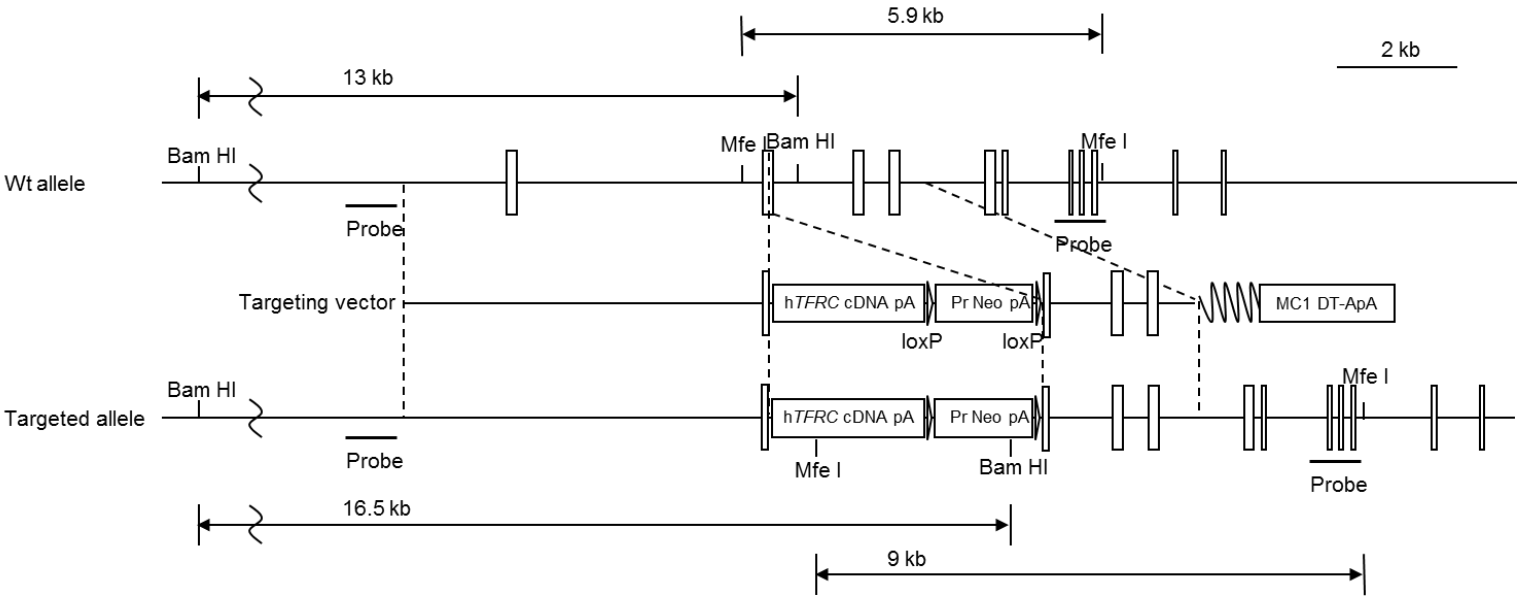

Figure S1. Schematic representation of mouse *Tfrc* gene, targeting vector, and targeted allele
A human *TFRC* cDNA cassette was inserted into exon 2 of the mouse *Tfrc* gene. Positive and negative clones can be discriminated by the DNA fragment size in Southern blot analysis after digestion with Bam HI or Mfe I.

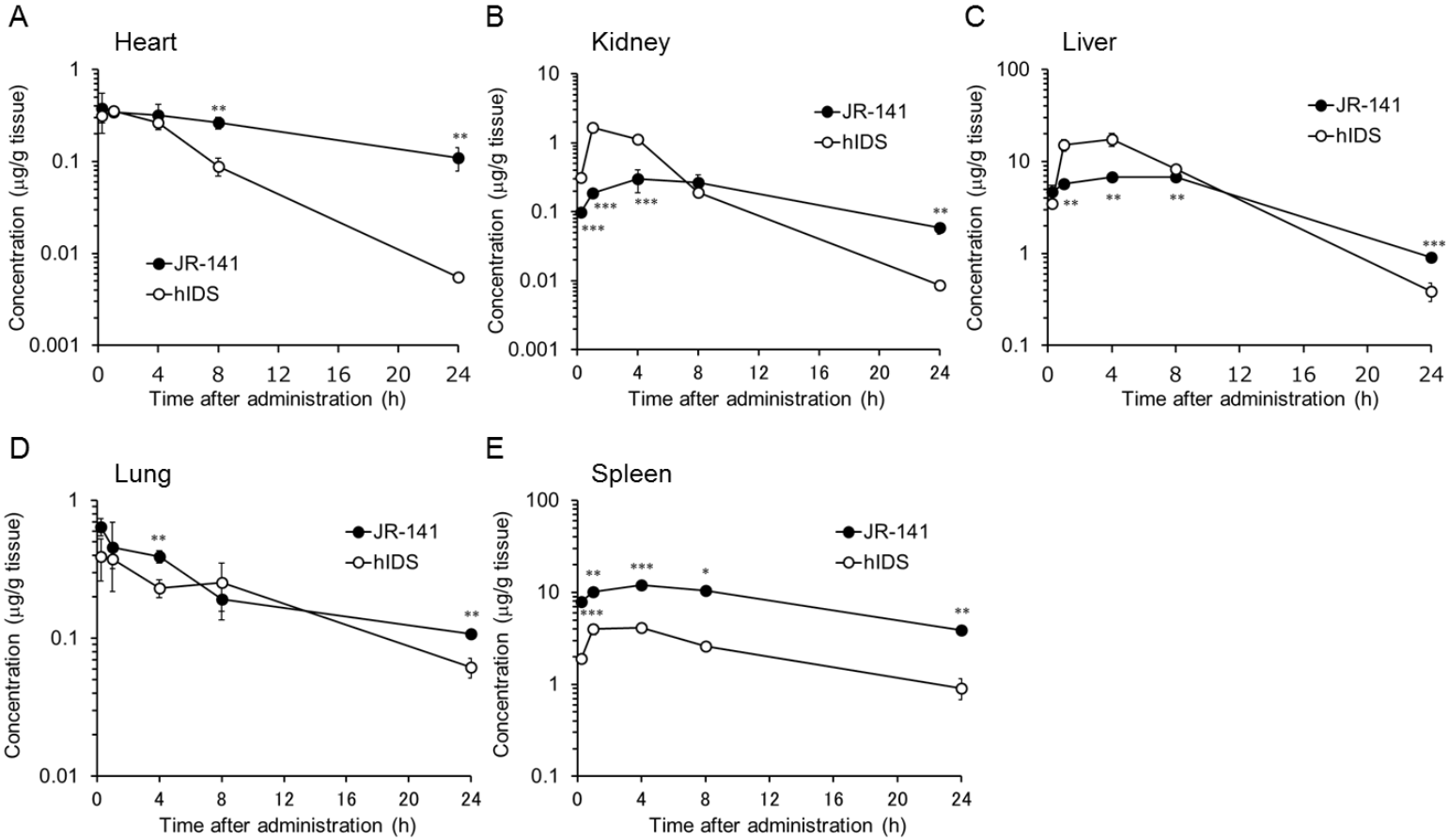

Figure S2. Pharmacokinetics of JR-141 and hIDS in peripheral tissues of *TFRC*-KI mice
Concentration of JR-141 was measured in the heart (A), kidney (B), liver (C), lung (D), and spleen (E) by electrochemiluminescent immunoassay (n = 3; **P* < 0.05, ***P* < 0.01, ****P* < 0.001, *t*-test). Data are plotted as mean ± SD bars.

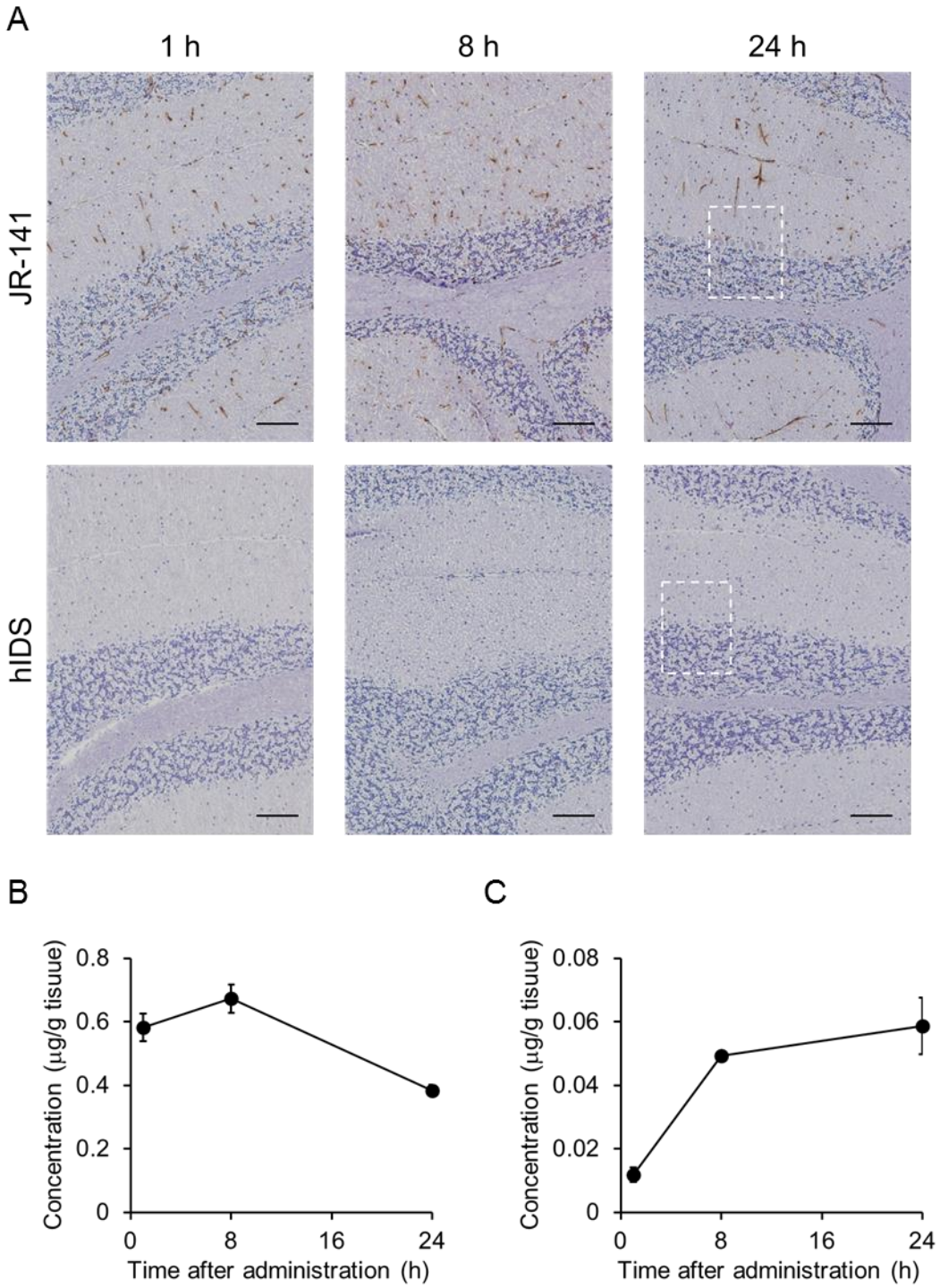

Figure S3. Immunohistochemistry in the brain of *TFRC*-KI mice
(A) Low magnification microphotographs of the cerebellum at 1, 8, 24 h after the administration of 1 mg/kg of JR-141 or naked IDS. White dashed rectangles indicate the highly magnified areas shown in Figure 3C. Scale bars, 100 μm. (B and C) Concentrations of JR-141 in brain capillaries (B) and parenchyma (C). Data are plotted as mean ± SD bars (n = 3).

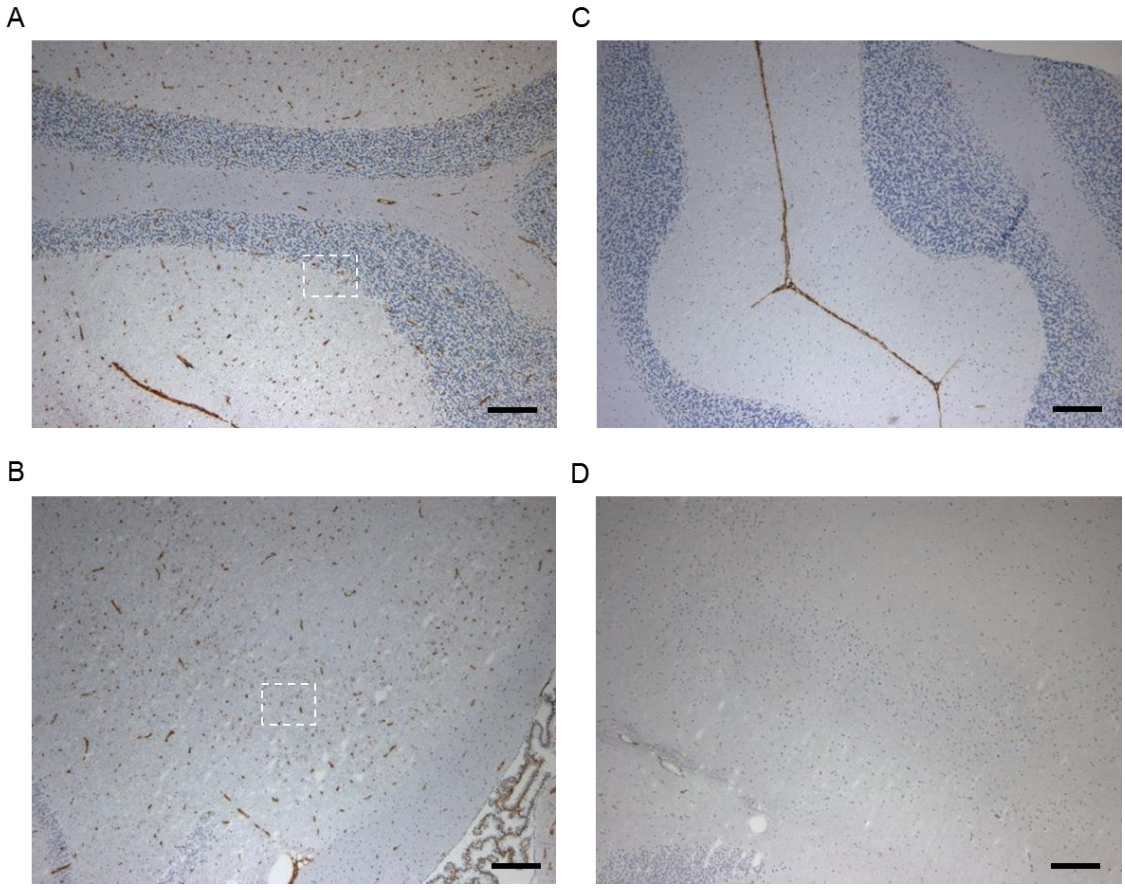

Figure S4. Immunohistochemistry in the brain of cynomolgus monkey
Representative brain sections from the JR-141 (5 mg/kg) group (A and B) and control (no administration) group (C and D). Low magnification microphotographs of the cerebellum (A and C) and the hippocampus (B and D) are shown. Non-specific staining is observed in the pia mater (C). White dashed rectangles indicate the highly magnified areas shown in Figures 4D and 4E. Scale bars, 200 μm.

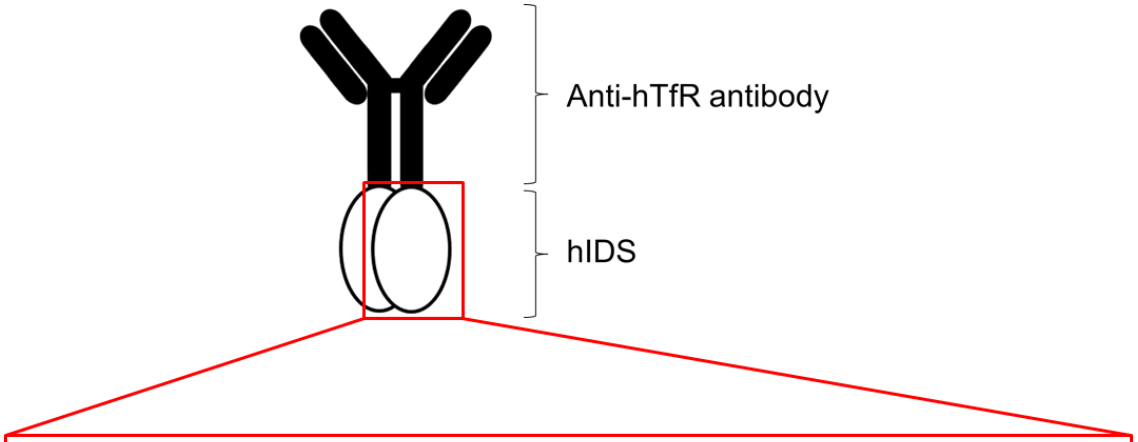

SETQANSTTD ALNVLLIIVD DLRPSLGCYG DKLVRSPNID QLASHSLLFQ
NAFAQQAVCA PSRVSFLTGR RPDTTRLYDF NSYWRVHAGN FSTIPQYFKE
NGYVTMSVGK VFHPGISSNH TDDSPYSWSF PPYHPSSEKY ENTKTCRGPD
GELHANLLCP VDVLDVPEGT LPDKQSTEQA IQLLEKMKTS ASPFFLAVGY
HKPHIPFRYP KEFQKLYPLE NITLAPDPEV PDGLPPVAYN PWMDIRQRED
VQALNISVPY GPIPVDFQRK IRQSYFASVS YLDTQVGRLL SALDDLQLAN
STIIAFTSDH GWALGEHGEW AKYSNFDVAT HVPLIFYVPG RTASLPEAGE
KLFPYLDPFD SASQLMEPGR QSMDLVELVS LFPTLAGLAG LQVPPRCPVP
SFHVELCREG KNLLKHFRFR DLEEDPYLPG NPRELIAYSQ YPRPSDIPQW
NSDKPSLKDI KIMGYSIRTI DYRYTVWVGF NPDEFLANFS DIHAGELYFV
DSDPLQDHNM YNDSQGGDLF QLLMP

Figure S5. The amino acid sequence of the hIDS moiety of JR-141 predicted from the cDNA sequence
N: N-glycosylation site

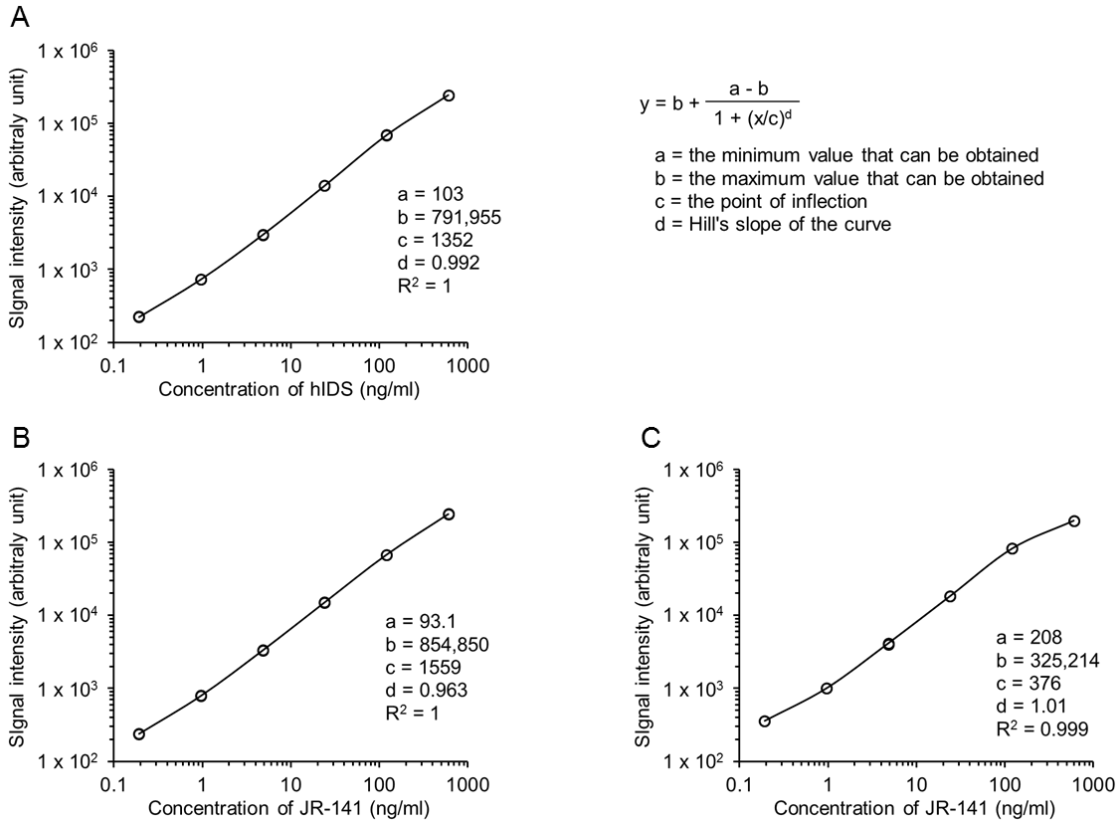

Figure S6. Validity of electrochemiluminescent immunoassay of hIDS and JR-141
(A) A representative standard curve for hIDS measurement. Defined concentrations of hIDS were added to the mixture of the sulfo-labeled anti-hIDS antibody and the biotinylated anti-hIDS antibody, and the reactions were then added to pre-blocked Streptavidin Gold plate (Meso Scale Diagnostics, Gaithersburg, MD). The intensity of electrochemiluminescence was quantified by Sector Imager 6000 (Meso Scale Diagnostics). (B and C) Representative standard curves for JR-141 measurement. Defined concentrations of JR-141 were mixed with biotinylated light chain of anti-human IgG antibody (B) or biotinylated anti-hIDS antibody (C) and SULFO-TAG-labeled anti-hIDS antibody. The subsequent procedure was similar to that described in (A). Four-parameter logistic regression was applied.

Table S1. Pharmacokinetic parameters of JR-141 and naked hIDS after intravenous administration to *TFRC*-KI mice

	Drug	C_{max} (μg/ml or g)	$AUC_{0\text{-}t}$ (μg·h/ml or g)	$AUC_{0\text{-}inf}$ (μg·h/ml or g)	$t_{1/2}$ (h)	MRT (h)	CL (ml/h/kg)	V_{ss} (ml/kg)
Plasma	JR-141	15.3	25.4	25.6	4.37	1.78	39.1	69.5
	hIDS	21.2	17.9	17.9	4.89	0.718	55.8	40.1
Brain	JR-141	0.440	8.14	16.6	23.9	34.9	60.4	2,110
	hIDS	-	-	-	-	-	-	-
Heart	JR-141	0.370	5.51	7.55	12.9	17.8	132	2,350
	hIDS	0.356	2.68	2.71	3.69	4.95	369	1,830
Kidney	JR-141	0.297	4.54	5.24	8.13	11.8	191	2,250
	hIDS	1.66	9.17	9.20	3.02	3.99	109	433
Liver	JR-141	6.82	112	120	5.51	8.85	8.36	74.0
	hIDS	17.4	177	179	3.64	5.97	5.58	33.3
Lung	JR-141	0.588	5.40	7.21	12.3	16.4	139	2,270
	hIDS	0.399	4.79	5.67	9.52	12.2	176	2,150
Spleen	JR-141	11.9	201	269	12.0	17.1	3.72	63.5
	hIDS	4.14	55.9	68.2	9.54	13.3	14.7	196

C_{max}; maximum concentration, $AUC_{0\text{-}t}$: area under the concentration-time curve from zero to the time of the last measurable drug concentration, $AUC_{0\text{-}inf}$: area under the concentration-time curve from zero to infinity, $t_{1/2}$: half-life, MRT: mean residence time, CL: clearance, V_{SS}: steady-state distribution volume.

Table S2. Pharmacokinetic parameters of JR-141 in plasma after intravenous administration to cynomolgus monkeys

C_{max} (μg/mL)	$AUC_{0\text{-}t}$ (μg·h/ml)	$AUC_{0\text{-}inf}$ (μg·h/ml)	$t_{1/2\beta}$ (h)	MRT (h)	CL (m1/h/kg)	V_{ss} (ml/kg)
75.4	446	424	4.69	6.25	12.2	74.1

C_{max}; maximum concentration, $AUC_{0\text{-}t}$: area under the concentration-time curve from zero to the time of the last measurable drug concentration, $AUC_{0\text{-}inf}$: area under the concentration-time curve from zero to infinity, $t_{1/2}$: half-life of β phase, MRT: mean residence time, CL: clearance, V_{SS}: steady-state distribution volume.

Table S3. Absolute values of concentration of GAG levels in the brain and peripheral tissues

		GAG (μg/mg tissue)																					
		Brain				Heart				Kidney				Liver				Lung				Spleen			
			mean	SD	*P* value		mean	SD	*P* value		mean	SD	*P* value		mean	SD	*P* value		mean	SD	*P* value		mean	SD	*P* value
Wilde-type		2.15 2.37 2.33 2.29	2.29	0.09	-	0.97 0.95 0.78 0.88	0.89	0.08	-	2.00 1.96 1.99 1.96	1.98	0.02	-	0.98 1.10 1.05 1.15	1.07	0.07	-	1.09 1.06 1.08 1.15	1.09	0.04	-	0.64 0.55 0.51 0.65	0.59	0.07	-
Ids-KO (Control)		3.14 3.05 3.01 3.24	3.11	0.10	-	4.89 6.22 5.57 5.83	5.63	0.56	-	11.65 11.98 12.43 11.82	11.97	0.33	-	14.95 19.16 15.67 13.00	15.69	2.57	-	7.40 7.28 7.02 6.67	7.09	0.32	-	4.65 4.54 3.91 5.82	4.73	0.79	-
JR-141	1 mg/kg	2.71 2.71 2.81 2.63	2.72	0.07	0.000053	2.00 2.05 2.26 1.82	2.03	0.18	4.54.E-08	8.67 8.09 7.79 6.06	7.65	1.13	0.000004	3.60 3.47 3.58 2.60	3.31	0.48	0.000028	5.83 6.16 6.33 5.66	5.99	0.31	0.005	1.76 1.52 1.51 1.50	1.57	0.13	0.000001
	3 mg/kg	2.50 2.39 2.40	2.43	0.06	5.77.E-07	1.66 1.62 1.65	1.64	0.02	4.26.E-08	5.07 4.17 4.15	4.46	0.52	6.78.E-08	3.69 2.68 3.19	3.19	0.50	4.33.E-07	4.94 3.98 3.93	4.28	0.57	0.000003	1.35 1.29 1.34	1.33	0.03	0.000001
	10 mg/kg	2.40 2.54 2.52 2.51	2.49	0.06	6.54.E-07	1.28 1.23 1.30 1.19	1.25	0.05	3.49.E-08	3.03 3.39 3.40 3.12	3.23	0.19	3.64.E-08	2.20 2.27 2.88 2.38	2.43	0.31	1.32.E-07	2.17 2.35 3.00 2.33	2.46	0.36	4.23.E-08	1.00 1.27 1.31 1.18	1.19	0.14	4.46.E-07
hIDS	0.5 mg/kg	3.11 3.07 2.94 2.80	2.98	0.14	0.179	1.50 1.54 1.36 1.64	1.51	0.11	0.000007	7.36 8.40 8.96 8.03	8.19	0.67	0.000055	4.27 3.50 3.61 3.79	3.79	0.34	0.000094	5.12 5.29 3.75 5.55	4.93	0.80	0.002	2.14 1.97 1.99 1.86	1.99	0.12	0.00049

Differences between *Ids*-KO control and JR-141 groups, and *Ids*-KO control and hIDS groups were analyzed with Dunnett's test and Student *t*-test, respectively.

SUPPLEMENTAL MATERIALS AND METHODS

Generation of *TFRC*-KI mice

TFRC-KI mice in a C57BL/6 background were generated by homologous recombination of the *TFRC* gene with the mouse *Tfrc* gene. A cDNA coding for a chimeric protein of the extracellular domain of human TFRC and the transmembrane and intracellular domain of mouse Tfrc was inserted into exon 2 of the mouse *Tfrc* gene (Figure S1). The nucleotide sequence of the cDNA with loxP-neo-loxP is shown below:

gtttatcctcccttgtagcagctgagaATGATGGATCAAGCCAGATCAGCATTCTCTAACTTGTTTGGTG
GGGAACCATTGTCATACACCCGGTTTAGCCTTGCTCGGCAAGTAGATGGAGATAACAGTCATGTGGAGAT
GAAACTGGCTGCAGATGAAGAAGAAAATGCCGACAATAACATGAAGGCTAGTGTCAGAAAACCCAAGAGG
TTTAATGGAAGACTCTGCTTTGCAGCTATTGCACTAGTCATTTTCTTCTTGATTGGATTCATGAGTGGCT
ACCTGGGCTATTGTAAAGGGGTAGAACCAAAAACTGAGTGTGAGAGACTGGCAGGAACCGAGTCTCCAGT
GAGGGAGGAGCCAGGAGAGGACTTCCCTGCAGCACGTCGCTTATATTGGGATGACCTGAAGAGAAAGTTG
TCGGAGAAACTGGACAGCACAGACTTCACCGGCACCATCAAGCTGCTGAATGAAAATTCATATGTCCCTC
GTGAGGCTGGATCTCAAAAAGATGAAAATCTTGCGTTGTATGTTGAAAATCAATTTCGTGAATTTAAACT
CAGCAAAGTCTGGCGTGATCAACATTTTGTTAAGATTCAGGTCAAAGACAGCGCTCAAAACTCGGTGATC
ATAGTTGATAAGAACGGTAGACTTGTTTACCTGGTGGAGAATCCTGGGGGTTATGTGGCGTATAGTAAGG
CTGCAACAGTTACTGGTAAACTGGTCCATGCTAATTTTGGTACTAAAAAAGATTTTGAGGATTTATACAC
TCCTGTGAATGGATCTATAGTGATTGTCAGAGCAGGGAAAATCACCTTTGCAGAAAAGGTTGCAAATGCT
GAAAGCTTAAATGCAATTGGTGTGTTGATATACATGGACCAGACTAAATTTCCCATTGTTAACGCAGAAC
TTTCATTCTTTGGACATGCTCATCTGGGGACAGGTGACCCTTACACACCTGGATTCCCTTCCTTCAATCA
CACTCAGTTTCCACCATCTCGGTCATCAGGATTGCCTAATATACCTGTCCAGACAATCTCCAGAGCTGCT
GCAGAAAAGCTGTTTGGGAATATGGAAGGAGACTGTCCCTCTGACTGGAAAACAGACTCTACATGTAGGA
TGGTAACCTCAGAAAGCAAGAATGTGAAGCTCACTGTGAGCAATGTGCTGAAAGAGATAAAAATTCTTAA
CATCTTTGGAGTTATTAAAGGCTTTGTAGAACCAGATCACTATGTTGTAGTTGGGGCCCAGAGAGATGCA
TGGGGCCCTGGAGCTGCAAAATCCGGTGTAGGCACAGCTCTCCTATTGAAACTTGCCCAGATGTTCTCAG
ATATGGTCTTAAAAGATGGGTTTCAGCCCAGCAGAAGCATTATCTTTGCCAGTTGGAGTGCTGGAGACTT
TGGATCGGTTGGTGCCACTGAATGGCTAGAGGGATACCTTTCGTCCCTGCATTTAAAGGCTTTCACTTAT
ATTAATCTGGATAAAGCGGTTCTTGGTACCAGCAACTTCAAGGTTTCTGCCAGCCCACTGTTGTATACGC
TTATTGAGAAAACAATGCAAAATGTGAAGCATCCGGTTACTGGGCAATTTCTATATCAGGACAGCAACTG
GGCCAGCAAAGTTGAGAAACTCACTTTAGACAATGCTGCTTTCCCTTTCCTTGCATATTCTGGAATCCCA
GCAGTTTCTTTCTGTTTTTGCGAGGACACAGATTATCCTTATTTGGGTACCACCATGGACACCTATAAGG
AACTGATTGAGAGGATTCCTGAGTTGAACAAAGTGGCACGAGCAGCTGCAGAGGTCGCTGGTCAGTTCGT
GATTAAACTAACCCATGATGTTGAATTGAACCTGGACTATGAGAGGTACAACAGCCAACTGCTTTCATTT
GTGAGGGATCTGAACCAATACAGAGCAGACATAAAGGAAATGGGCCTGAGTTTACAGTGGCTGTATTCTG
CTCGTGGAGACTTCTTCCGTGCTACTTCCAGACTAACAACAGATTTCGGGAATGCTGAGAAAACAGACAG
ATTTGTCATGAAGAAACTCAATGATCGTGTCATGAGAGTGGAGTATCACTTCCTCTCTCCCTACGTATCT
CCAAAAGAGTCTCCTTTCCGACATGTCTTCTGGGGCTCCGGCTCTCACACGCTGCCAGCTTTACTGGAGA
ACTTGAAACTGCGTAAACAAAATAACGGTGCTTTTAATGAAACGCTGTTCAGAAACCAGTTGGCTCTAGC
TACTTGGACTATTCAGGGAGCTGCAAATGCCCTCTCTGGTGACGTTTGGGACATTGACAATGAGTTTTAA
cgtGGCTCGCTGATCAGCCTCGACTGTGCCTTCTAGTTGCCAGCCATCTGTTGTTTGCCCCTCCCCCGTG
CCTTCCTTGACCCTGGAAGGTGCCACTCCCACTGTCCTTTCCTAATAAAATGAGGAAATTGCATCGCATT
GTCTGAGTAGGTGTCATTCTATTCTGGGGGGTGGGGTGGGGCAGGACAGCAAGGGGGAGGATTGGGAAGA
CAATAGCAGGCATGCTGGGGATGCGGTGGGCTCTATGGCTTCTGAGGCGGAAAGAACCAGCTGGGGCTCG
ATCCTCTAGTTaagcttcccagcggccgctatcgaattccgatcatattcaataacccttaatATAACTT
CGTATAATGTATGCTATACGAAGTTATtaggtctgaagaggagtttacgtccagccaagctAATTCTACC
GGGTAGGGGAGGCGCTTTTCCCAAGGCAGTCTGGAGCATGCGCTTTAGCAGCCCCGCTGGGCACTTGGCG
CTACACAAGTGGCCTCTGGCCTCGCACACATTCCACATCCACCGGTAGGCGCCAACCGGCTCCGTTCTTT
GGTGGCCCCTTCGCGCCACCTTCTACTCCTCCCCTAGTCAGGAAGTTCCCCCCCGCCCCGCAGCTCGCGT
CGTGCAGGACGTGACAAATGGAAGTAGCACGTCTCACTAGTCTCGTGCAGATGGACAGCACCGCTGAGCA
ATGGAAGCGGGTAGGCCTTTGGGGCAGCGGCCAATAGCAGCTTTGCTCCTTCGCTTTCTGGGCTCAGAGG
CTGGGAAGGGGTGGGTCCGGGGGCGGGCTCAGGGGCGGGCTCAGGGGCGGGGCGGGCGCCCGAAGGTCCT
CCGGAGGCCCGGCATTCTGCACGCTTCAAAAGCGCACGTCTGCCGCGCTGTTCTCCTCTTCCTCATCTCC
GGGCCTTTCGAcctgcagccaatATGGGATCGGCCATTGAACAAGATGGATTGCACGCAGGTTCTCCGGC
CGCTTGGGTGGAGAGGCTATTCGGCTATGACTGGGCACAACAGACAATCGGCTGCTCTGATGCCGCCGTG
TTCCGGCTGTCAGCGCAGGGGCGCCCGGTTCTTTTTGTCAAGACCGACCTGTCCGGTGCCCTGAATGAAC
TGCAGGACGAGGCAGCGCGGCTATCGTGGCTGGCCACGACGGGCGTTCCTTGCGCAGCTGTGCTCGACGT
TGTCACTGAAGCGGGAAGGGACTGGCTGCTATTGGGCGAAGTGCCGGGGCAGGATCTCCTGTCATCTCAC
CTTGCTCCTGCCGAGAAAGTATCCATCATGGCTGATGCAATGCGGCGGCTGCATACGCTTGATCCGGCTA
CCTGCCCATTCGACCACCAAGCGAAACATCGCATCGAGCGAGCACGTACTCGGATGGAAGCCGGTCTTGT
CGATCAGGATGATCTGGACGAAGAGCATCAGGGGCTCGCGCCAGCCGAACTGTTCGCCAGGCTCAAGGCG
CGCATGCCCGACGGCGAGGATCTCGTCGTGACCCATGGCGATGCCTGCTTGCCGAATATCATGGTGGAAA

ATGGCCGCTTTTCTGGATTCATCGACTGTGGCCGGCTGGGTGTGGCGGACCGCTATCAGGACATAGCGTT
GGCTACCCGTGATATTGCTGAAGAGCTTGGCGGCGAATGGGCTGACCGCTTCCTCGTGCTTTACGGTATC
GCCGCTCCCGATTCGCAGCGCATCGCCTTCTATCGCCTTCTTGACGAGTTCTTCTGAGgggatccgctgt
aagtctgcagaaattGATGATCTATTAAACAATAAAGATGTCCACTAAAATGGAAGTTTTTCCTGTCATA
CTTTGTTAAGAAGGGTGAGAACAGAGTACCTACATTTTGAATGGAAGGATTGGAGCTACGGGGGTGGGGG
TGGGGTGGGATTAGATAAATGCCTGCTCTTTACTGAAGGCTCTTTACTATTGCTTTATGATAATGTTTCA
TAGTTGGATATCATAATTTAAacaagcaaaaccaaattaagggccagctcattcctcccactcatgatct
atagatccctcgatcgagatccggaacccttaatATAACTTCGTATAATGTATGCTATACGAAGTTATta
ggtccctcgaagaggttcactagttctagagcatttaaatacgtgctagc

Boxed letters indicate the cDNA for the chimeric receptor and underlines indicate loxP sequences. The expression pattern of TfR in *TFRC*-KI mice was qualitatively similar to that in WT mice.